

PAPER • OPEN ACCESS

Dynamic performance of arc-shaped auxetic structures through split Hopkinson pressure bar tests

To cite this article: Ehsan Etemadi *et al* 2025 *Smart Mater. Struct.* **34** 085022

View the [article online](#) for updates and enhancements.

You may also like

- [Optimization design and performance analysis of pneumatic grid flexible actuator](#)
Yonglin Zhong, Yuanhao Cheng, Si Chen et al.
- [Enhancing vitrimer applications: development of E-GMA/EMAZn vitrimeric filaments for advanced 3D/4D printing](#)
Rafael Braga da Cunha, Jaini Miscilene de Araújo, Válmer Azevedo de Sousa Filho et al.
- [Unidirectional torsional T\(0,1\) wave meta-transducer for circumferential-axial defect localization in pipes](#)
Yuehao Du, Gang Wang and Hongchen Miao



The banner features a blue background with a large white circle on the left containing the '250' logo. The '2' is red, the '5' is blue, and the '0' is green. A blue ribbon with 'ECS MEETING CELEBRATION' is wrapped around the '0'. To the right of the circle, the ECS logo and name are displayed. The right side of the banner has a green background with white text and a red button.

ECS The Electrochemical Society
Advancing solid state & electrochemical science & technology

*Step into the
Spotlight*

**SUBMIT YOUR
ABSTRACT**

250th ECS Meeting
October 25–29, 2026
Calgary, Canada
BMO Center

Submission deadline:
March 27, 2026

Dynamic performance of arc-shaped auxetic structures through split Hopkinson pressure bar tests

Ehsan Etemadi^{1,2} , Mahbubeh Hosseinabadi³, Mohaddeseh Gholikord¹,
Mohammad Abbaslou³, Mohammad Imani¹ and Hong Hu^{2,*} 

¹ Department of Mechanical Engineering, Hakim Sabzevari University, Sabzevar, Iran

² School of Fashion & Textiles, The Hong Kong Polytechnic University, Hong Kong, People's Republic of China

³ School of Mechanical Engineering, Iran University of Science and Technology, Tehran, Iran

E-mail: hu.hong@polyu.edu.hk

Received 11 June 2025, revised 23 July 2025

Accepted for publication 7 August 2025

Published 20 August 2025



Abstract

This study investigates the mechanical behavior of auxetic energy-absorbing structures with arc-shaped members under dynamic loading. Four configurations namely RED, Multiple-Arc, REC-Star, and REC-Flower were designed and evaluated. The Multiple-Arc and RED structures were fabricated using fused deposition modeling and tested via Split Hopkinson Pressure Bar experiments, while all structures were analyzed using finite element modeling. The experimental results demonstrated good agreement with numerical simulations, validating the accuracy of the FE approach. Also, the energy absorption (EA), specific energy absorption (SEA), and Poisson's ratio of the structures were compared. The Multiple-Arc structure exhibited the highest EA and SEA due to its arc-shaped internal members, which enhanced stress transfer and impact dissipation. The REC-Flower structure also performed well, benefiting from curved members that reduced stress concentration. Conversely, the RED structure, lacking internal members, showed the lowest EA due to inefficient wave transmission. The REC-Star structure initially displayed high EA but experienced premature failure due to stress concentration at sharp corners. These findings emphasize the significance of curved internal member arrangement in optimizing auxetic structures for dynamic applications. The results provide insights into designing auxetic materials with tailored EA and deformation characteristics for impact-resistant applications.

Supplementary material for this article is available [online](#)

Keywords: negative Poisson's ratio, curved auxetic structures, split Hopkinson pressure bar, energy absorption, fused deposition modeling, finite element method

* Author to whom any correspondence should be addressed.



Original content from this work may be used under the terms of the [Creative Commons Attribution 4.0 licence](#). Any further distribution of this work must maintain attribution to the author(s) and the title of the work, journal citation and DOI.

1. Introduction

Auxetic structures are a group of metamaterials that exhibit unique behaviors due to their negative Poisson's ratio. Unlike conventional materials that shrink (expand) laterally under tensile (compressive) loading, auxetic structures expand (shrink) in the lateral direction due to applied tension (compression). This behavior is achieved through the unique design of their cellular structure. The negative Poisson's ratio behavior in auxetic structures enhances mechanical properties, making them superior compared to conventional materials and structures. These superior properties include remarkable energy absorption (EA) [1–8], load-bearing capability [9–13], fracture toughness [14–17], high indentation resistance [18–21], and thermal impact resistance [22–25]. Such properties enable a wider range of applications for auxetic structures in various fields, including mechanical [26–32], medical [27, 33–40], sports [41–44], and textile [45–49] industries.

Recently, arc-shaped auxetic structures have been explored through innovative design and modification of conventional auxetic structures by replacing straight members with arc-shaped struts in unit cells, such as re-entrant cells under quasi-static [50–54] and dynamic loadings [55, 56]. Designing novel arc-shaped unit cells have been developed to increase EA capacity and reduce stress concentration in these structures [57]. For example, Qi *et al* [54] developed a new re-entrant unit cell with double circular members instead of the traditional inclined members. Their experimental and finite element (FE) analysis demonstrated that these circular re-entrant auxetic structures absorbed more energy than conventional re-entrant structures under quasi-static compression loading. Etemadi *et al* [2] designed three novel auxetic structures by replacing straight members with curved ones in the re-entrant unit cell, evaluating the behavior of these 3D printed structures under quasi-static compression loading. They found that the EA values in curved-shaped re-entrant structures significantly exceeded those of the conventional re-entrant structure. In another study, Etemadi *et al* [58] introduced two types of arc-shaped auxetic structures as a new generation of auxetic structures, concluding their structures exhibited higher EA capacity than conventional auxetic structures under quasi-static compressive loading.

Furthermore, auxetic structures with arc shaped members exhibit exceptional behavior under dynamic loading due to reduced stress concentration and more uniform stress distribution, which contribute increased resistance and structural stability [2, 58–61]. Fu *et al* [62] investigated a sandwich structure with Arc-type auxetic core under impact loading demonstrating that the auxetic core with arc shaped members increases the structure's EA capacity. Hao *et al* [63] introduced novel arc-shaped structures to further improve EA capacity under dynamic loading, with numerical and theoretical results indicating that arc-shaped members reduce stress concentration and increase EA.

The split Hopkinson pressure bar (SHPB) is a testing device that enables researchers to evaluate and study the performance of materials and structures under medium to high strain rates.

Hopkinson first established the foundation of this method in 1914 [64], and in 1949, Kolsky [65] modified it by using two bars in series, presenting a technique for measuring the stress–strain relationship of materials under high-rate loading, known as the SHPB.

Unlike drop-weight testing machines, which are commonly used for low-velocity impact loading [9, 60, 66, 67], the SHPB is specifically employed to evaluate the mechanical behavior of auxetic structures under high strain rate loading [59, 68–72]. Fila *et al* [73] subjected three types of auxetic structures, including 2D missing rib, 2D re-entrant, and 3D re-entrant filled with strain rate sensitive materials, to quasi-static and SHPB tests, investigating the effect of loading rate on their mechanical properties. The results indicated that the effect of polyurethane foam filling on specific energy absorption (SEA) in dynamic loading was 15% higher than under quasi-static loading. Chen *et al* [74] subjected five types of 3D re-entrant structures with different geometries made of polyamide to SHPB impact tests at various velocities, comparing stress–strain curves, EA, and failure mode under impact loading, were compared with the quasi-static test results. They found results that strength and EA abilities during impact loading were significantly improved compared to quasi-static loading tests. Varas *et al* [75] developed a new 3D auxetic structure fabricated using additive manufacturing technology to investigate its mechanical behavior under different loading rates, employing the SHPB test for high-rate loading, and indicating that the EA value depends on the number of cell layers in the auxetic structure.

Auxetic structures have gained significant attention for applications related to EA under dynamic loading. However, most previous research has focused on traditional auxetic structures, leaving the behavior of arc-shaped auxetic structures under dynamic loading largely unexplored. This gap in the literature presents a significant deficiency in understanding how arc-shaped auxetic structures perform under impact loading.

In this research, four different arc-shaped auxetic structures were designed specifically to enhance their EA capacity under dynamic loading conditions. After fabricating these structures using additive manufacturing, they were subjected to SHPB tests to assess their mechanical performance and EA characteristics under impact loading with the results compared to finite element modeling (FEM) simulations. The primary aim of this study is to explore the behavior of arc-shaped auxetic structures and evaluate their EA and SEA under dynamic loading, providing valuable insights into their potential use as efficient energy-absorbing structures in engineering applications.

2. Designing approach

This study investigates impact loading of five arc-shaped auxetic structures designed to compare their EA capability. Figure 1 illustrates the designed structures along with their geometric parameter values, which were modified based on the geometric configuration of the REC structure (figure 1(a)) [54]. The REC structure was designed by replacing double

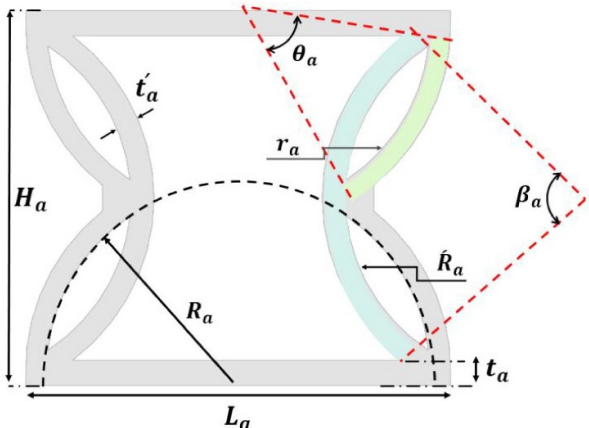
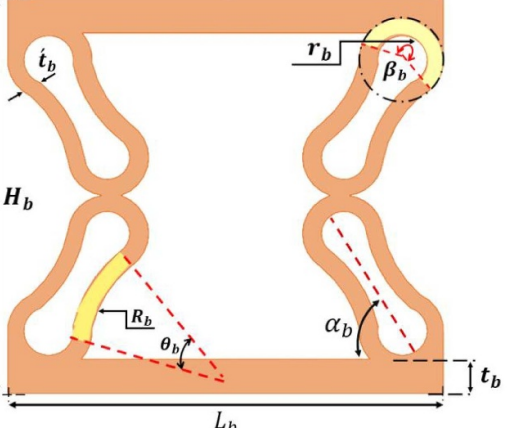
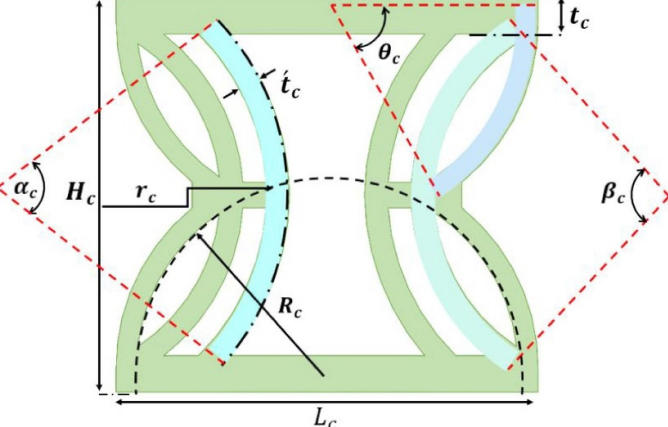
	Structure	Parameters
(a)	 <p>REC</p>	$H_a = 12.4mm$ $L_a = 12.9mm$ $R_a = 5.8mm$ $R'_a = 5.5mm$ $r_a = 5.6mm$ $t'_a = 10mm$ $\theta_a = 50^\circ$ $\beta_a = 75^\circ$
(b)	 <p>RED</p>	$H_b = 14.2mm$ $L_b = 14.2mm$ $R_b = 3.7mm$ $r_b = 0.9mm$ $t_b = 1.6mm$ $t'_b = 1mm$ $\theta_b = 35^\circ$ $\alpha_b = 60^\circ$ $\beta_b = 260^\circ$
(c)	 <p>Multiple-Arc</p>	$H_c = 12.3mm$ $L_c = 12.8mm$ $R_c = 5.8mm$ $r_c = 7.16mm$ $t_c = 1.12mm$ $t'_c = 1.1mm$ $q_c = 50^\circ$ $a_c = 75^\circ$ $b_c = 75^\circ$

Figure 1. Geometric parameters of the designed structures.

circular arcs with inclined members in re-entrant unit cells to reduce stress concentration and enhance mechanical behavior.

The designed structures include RED (figure 1(b)), Multiple-Arc (figure 1(c)), REC-Star (figure 1(d)), REC-Flower (figure 1(e)).

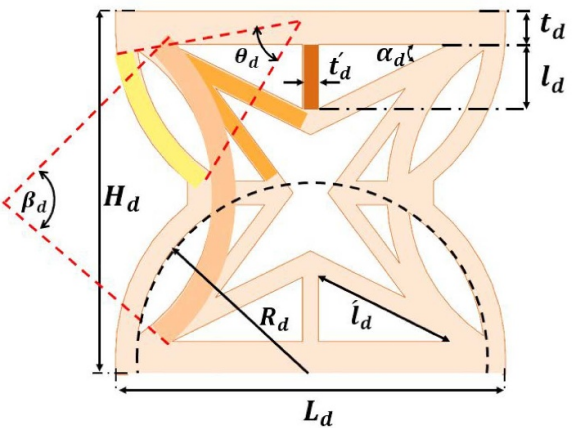
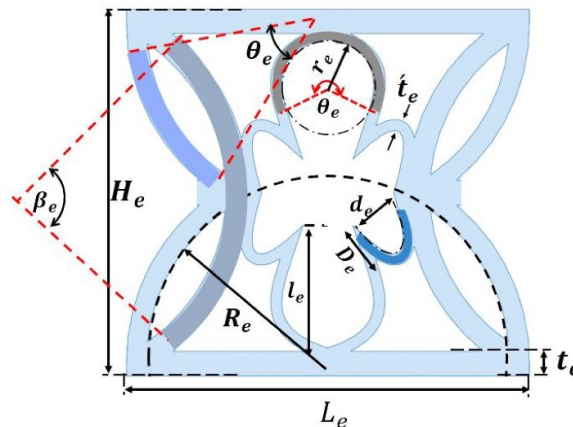
(d)		$H_d = 12.3mm$ $L_d = 13mm$ $l_d = 2.15mm$ $l'_d = 4.5mm$ $R_d = 5.8mm$ $t_d = 1.12mm$ $t'_d = 0.8mm$ $\theta_d = 50^\circ$ $\alpha_d = 26^\circ$ $\beta_d = 75^\circ$
(e)		$H_e = 12.3mm$ $L_e = 12.9mm$ $l_e = 4.7mm$ $R_e = 5.8mm$ $r_e = 2.7mm$ $t_e = 1.1mm$ $t'_e = 0.7mm$ $D_e = 1.8mm$ $d_e = 1.7mm$ $\theta_e = 50^\circ$ $\beta_e = 75^\circ$

Figure 1. (Continued.)

1. RED auxetic structure (figure 1(b)): This auxetic structure was developed by substituting the inclined re-entrant members with Dumbbell-shaped ones to achieve a higher negative Poisson's ratio and SEA. The RED structure is expected to exhibit superior auxetic behavior during impact loading due to the presence of its Dumbbell-shaped auxetic members.
2. Multiple-Arc auxetic structure (figure 1(c)): In this design, curved-arc members were added to the side walls of the REC unit cell to enhance its energy dissipation capabilities under compressive loads.
3. REC-Star structure (figure 1(d)): This structure combines auxetic star-shaped and REC designs. Given that the star-shaped energy-absorbing structures have high relative density, they are anticipated to have improved EA ability.
4. REC-Flower structure (figure 1(e)), the Flower unit cell was integrated within the REC unit cell. Due to the geometric configuration of the Flower auxetic unit cell, which avoids sharp corners, it is expected to demonstrate enhanced EA capability and auxetic behavior.

$$\Delta\rho_{\text{REC}} = \frac{\rho_o}{\rho_s} = \frac{4 \left[\frac{\theta_a}{2} \left((r_a + i_a)^2 - r_a^2 \right) \right] + 2 \left[\frac{\beta_a}{2} \left((R_a + i_a)^2 - R_a^2 \right) \right] + 2L_a t_a}{L_a H_a} \quad (1)$$

$$\Delta\rho_{\text{RED}} = \frac{\rho_o}{\rho_s} = \frac{4 \left[\theta_b \left((R_b + i_b)^2 - R_b^2 \right) \right] + 4 \left[\beta_b \left((r_b + i_b)^2 - r_b^2 \right) \right] + 2L_b t_b}{L_b H_b} \quad (2)$$

$$\Delta\rho_{\text{Multiple-Arc}} = \frac{\rho_o}{\rho_s} = \Delta\rho_{\text{REC}} + \frac{\alpha_c \left((\dot{R}_c + i_c)^2 - \dot{R}_c^2 \right)}{L_c H_c} \quad (3)$$

$$\Delta\rho_{\text{REC-Star}} = \frac{\rho_o}{\rho_s} = \Delta\rho_{\text{REC}} + \frac{2 \left[l_d i_d + 4 i_d t_d \right]}{L_d H_d} \quad (4)$$

$$\Delta\rho_{\text{REC-Flower}} = \Delta\rho_{\text{REC}} + \frac{2 \left[\frac{\theta_e}{2} \left((r_e + i_e)^2 - r_e^2 \right) \right] + \pi \left((r_e + i_e)^2 - r_e^2 \right)}{L_e H_e} \quad (5)$$

According to figures 1(a)–(e), the relative densities of five structures were approximately summarized as follows:

In this study, the geometric parameter values were selected to ensure that the relative densities of all structures were equal

to 0.6. This selection aimed to provide uniform conditions for comparing the mechanical behavior of the structures.

3. Experimental tests

3.1. Sample preparation

Among the five designed structures, the RED and Multiple-Arc structures were manufactured using a MakerBot fused deposition modeling (FDM) 3D printer with a 0.4 mm diameter nozzle. MakerBot ABS filament, known for its enhanced flexibility and acceptable ultimate strength, was selected as the 3D printing material. Table 1 provides detailed information on the 3D printing parameters used for fabricating the samples. In addition, figure 2 shows the printed samples.

Standard cylindrical samples with a diameter of 5 mm and a length of 11 mm were also manufactured to measure the mechanical properties of the parent material (ABS) under medium and high strain rate conditions, following the ASTM E2448-11 standard using the SHPB test [76]. The stress–strain diagrams of the ABS material obtained from three SHPB test results is shown in figure 3.

3.2. Split Hopkinson pressure bar

Dynamic experimental tests were performed using the SHPB machine installed at Hakim Sabzevari University. In designed SHPB set-up, two different types of steel bars are employed to measure the mechanical behavior of high strength materials, such as metals and high-strength composites. For materials with relatively lower strength, such as polymers and softer composites, aluminum bars are used. Using two types of bars allows accurate testing of various materials and helps precisely evaluate their behavior under different strain rates.

In this study, aluminum input and output bars with a length of 2 m and a diameter of 20.4 mm, along with a striker bar measuring 27 cm in length and 19.9 mm in diameter, a pressure supply system, a measuring system, and speedometers. Figures 4 and 5 show a schematic of the SHPB and the device located at Hakim Sabzevari University, respectively. Four strain gauges are installed at a distance of one meter from the input and output bar ends to measure the test outputs. Among the designed structures, the Multiple-Arc and RED structures were subjected to SHPB dynamic tests. The experimental deformation process for Multiple-Arc is documented in a supplementary video file.

The velocity of the striker bar in the SHPB test is measured using a laser system. This system detects changes in the position of a reflective surface on the striker bar, allowing the velocity to be calculated as:

$$V = \frac{\Delta x}{\Delta t} \quad (6)$$

where Δx is the displacement and Δt is the time interval between reflections. In this study, the striker bar velocity for both samples was measured at $14 \text{ m s}^{-1} \pm 0.5 \text{ m s}^{-1}$.

Table 1. 3D printing parameters for fabricated samples.

Material	ABS
Build orientation	Lay flat
Infill pattern	Linear
Infill density (%)	100
Layer thickness (mm)	0.2
Raster width (mm)	0.55
Nozzle diameters (mm)	0.4
Filament diameter (mm)	1.75
Print speed (mm/s)	50
Extrusion temperature ($^{\circ}\text{C}$)	245
Platform temperature ($^{\circ}\text{C}$)	93

The experimental test device operates as follows: initially, using the pressure supply system, the striking bar is accelerated to a velocity ranging from 0 to 40 meters per second. Upon impact with the input bar, a pressure wave propagates through the input bar to reach the structure. Due to the impedance difference between the two materials, a tensile wave is reflected back in the input bar, while a compression wave propagates through the output bar. With strain gauges installed on both the input and output bars, along with the measurement system, it is possible to measure the initial strain (ε_I), the strain reflected in the input bar (ε_R), and the transmitted strain through the output bar (ε_T). Using the values of these strains and equations (7)–(9), stress, strain, and strain rate can be calculated [77]:

$$\dot{\varepsilon}_s(t) = \frac{2c_b}{h_s} \varepsilon_R(t) \quad (7)$$

$$\varepsilon_s(t) = \frac{-2c_b}{h_s} \int_0^t \varepsilon_R(t) dt \quad (8)$$

$$\sigma(t) = \frac{A_b E_b}{A_s} \varepsilon_T \quad (9)$$

where c_b is the velocity of wave propagation, and E_b , A_b are the Young's modulus and cross-sectional area of the input bar, respectively. Additionally, A_s and h_s are the cross-sectional area and length of the auxetic sample, respectively. The EA and SEA of the auxetic samples were evaluated using equations (10) and (11):

$$EA = \int_0^{\varepsilon} \sigma(\varepsilon) d\varepsilon \quad (10)$$

$$SEA = \frac{EA}{\Delta \rho_s} \quad (11)$$

where ρ_s is the density of the parent material.

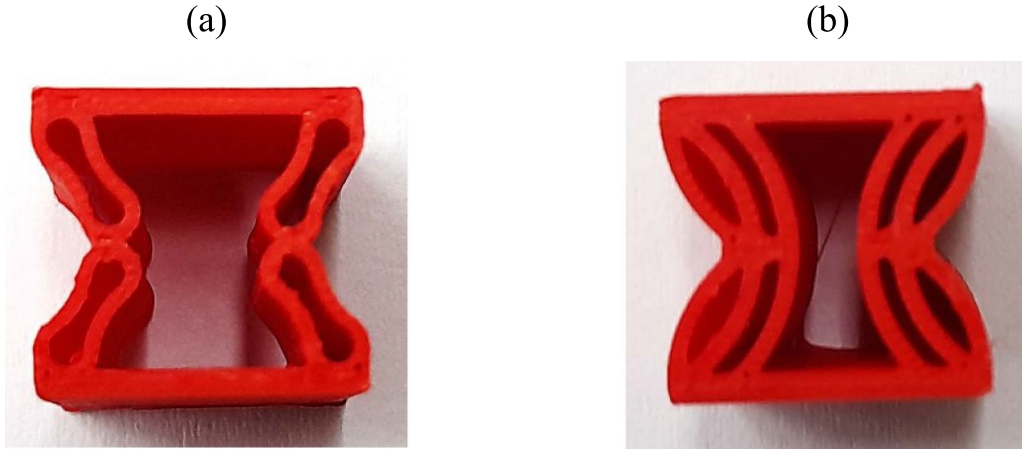


Figure 2. Printed samples: (a) RED, and (b) Multiple-Arc structures.

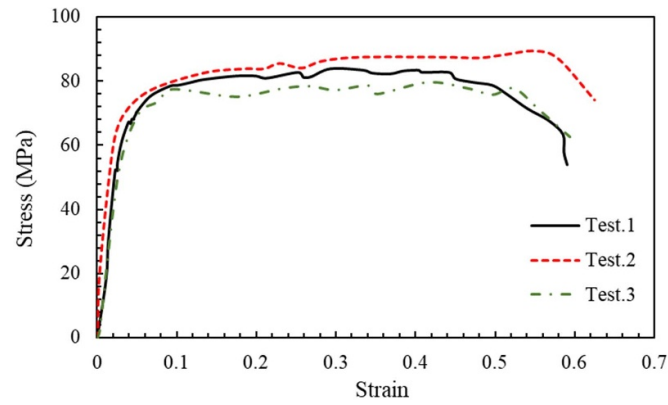


Figure 3. Stress–strain diagram of ABS material obtained from SHPB tests.

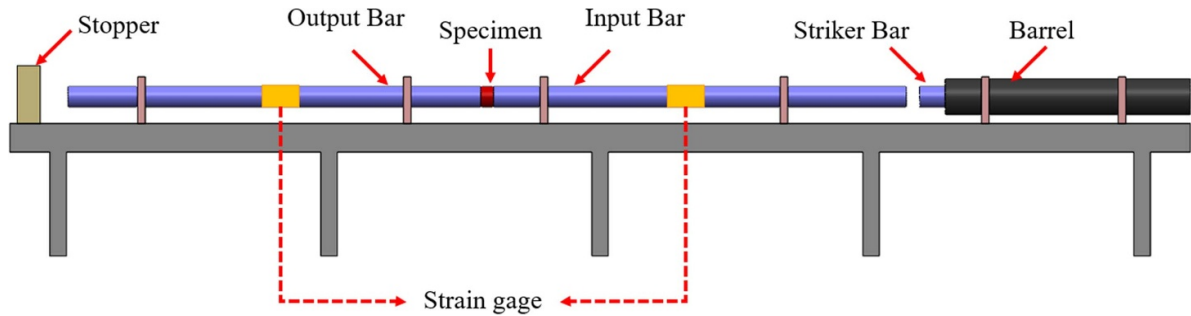


Figure 4. Schematic of the SHPB set-up.

4. Finite element method

In this section, the simulation process of the SHPB using FEM with Abaqus software was described. Abaqus is a commercial FE analysis software developed by Dassault Systèmes Simulia Corp., a subsidiary of Dassault Systèmes SE, headquartered in Vélizy-Villacoubly [78]. This software has been frequently used to evaluate the mechanical performance of materials and structures under high strain rate loading [79–82]. The exact specifications and dimensions of the pressure bars were modeled for the SHPB simulation, as shown in figure 6.

An elastic model was used for the input and output bars, and an elastic-plastic material model was implemented for the parent material of the designed auxetic samples. The mechanical properties of ABS were obtained based on the average stress–strain curves from three tests shown in figure 3 and are summarized in table 2, which also includes the mechanical properties of the bars.

C3D8R linear elements were used to mesh the bars and samples, as they are suitable for modeling large deformations and dynamic loadings, offering a good balance between computational efficiency and accuracy. Figure 7 shows a cut view of the bars and the structure meshing. To investigate the mesh



Figure 5. Two views of the SHPB device installed at Hakim Sabzevari University.

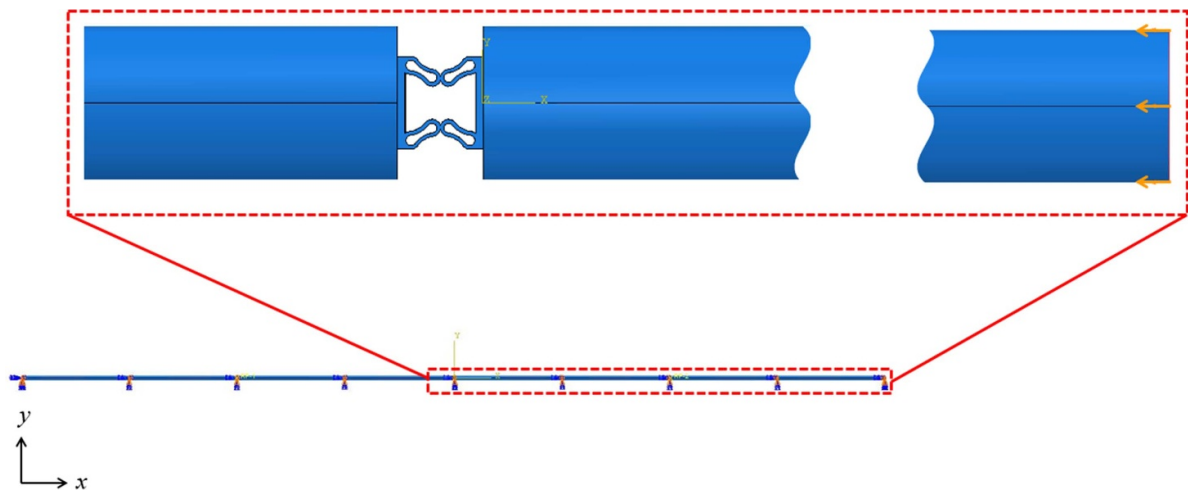


Figure 6. Schematic of the SHPB simulation.

Table 2. Mechanical properties of aluminum bars and ABS samples.

E_{Al} (GPa)	70
ρ_{Al} (kg/m ³)	2793
E_{ABS} (GPa)	2.40
$\rho_s = \rho_{ABS}$ (kg/m ³)	1130
ABS	0.33

sensitivity, as shown in figure 8, an initial element size (e.s.) of 0.4 mm was selected for the RED structure, and its stress–strain curve was evaluated. The element size was then reduced stepwise until further reduction did not significantly change the stress–strain curve. Based on this analysis, an element size of 0.15 mm was identified as the reference element size for the RED structure. The same approach was applied to the other structures.

Abaqus/ Explicit provides two contact algorithms for simulating interactions between different parts of the model: the general contact algorithm and the contact pair algorithm. The default general contact algorithm was employed in this study to capture all possible contact interactions during the

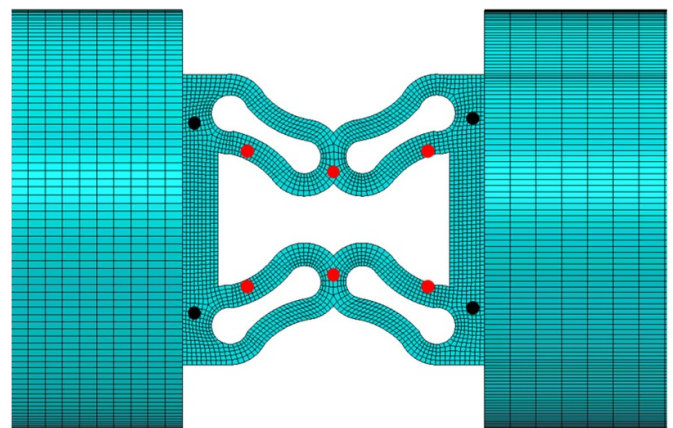


Figure 7. Cut view of the meshing of the input and output bars and the structure, along with the selection of red and black point pairs to evaluate lateral and axial displacements in the RED structure.

impact process automatically. This algorithm utilizes the penalty method to enforce contact constraints between surfaces, with a friction coefficient of 0.25 considered for tangential

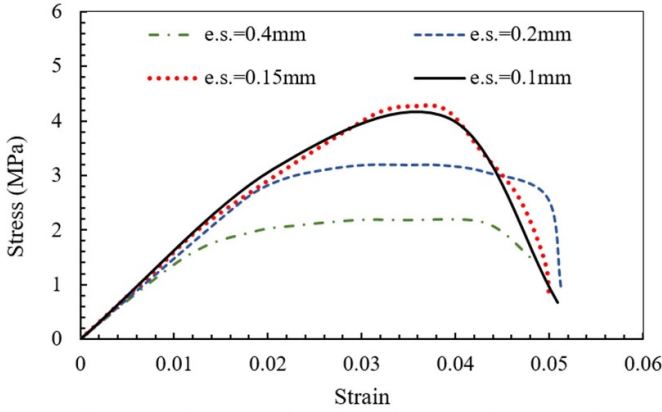


Figure 8. Mesh sensitivity analysis of the RED structure.

behavior [83]. The boundary conditions for the SHPB setup were applied to constrain all displacements in the bars except in the direction of the applied velocity. The simulation was carried out using a dynamic explicit solver, which is well-suited for modeling dynamic loading.

To evaluate Poisson's ratio of the RED structure, as shown in figure 7, pairs of horizontal [42] and vertical (black) nodes were selected to measure the average lateral (ε_y) and axial (ε_x) strains. Then, the Poisson's ratio was then calculated using equation (12)

$$\nu = -\frac{\varepsilon_y}{\varepsilon_x}. \quad (12)$$

5. Results and discussion

5.1. Comparison of experimental and FEM results

Figures 9 (a) and (b) present the stress–strain diagrams for the Multiple-Arc and RED structures, obtained from three times dynamic experimental tests and FEM, respectively. In addition, table 3 shows the ultimate strength (σ_u) values and their error percentage for experimental tests and FEM for the Multiple-Arc and RED auxetic structures. From figure 9 and table 3, the experimental and FEM results show good agreement. The discrepancies between the experimental and FEM results can be attributed to several factors. One main reason for differences is imperfections in the 3D printing process. These include small defects and slight geometric deviations. Such imperfections are not modeled in the FE simulations, which assume perfect bonding between structure members. Additionally, errors may arise from the SHPB experimental setup, including potential misalignments and frictional effects during loading, which could influence the accuracy of the measured results. Furthermore, material properties in the FEM model are typically considered homogeneous and isotropic, while the actual printed materials might exhibit anisotropic behavior or variability due to the layer-by-layer manufacturing process [84].

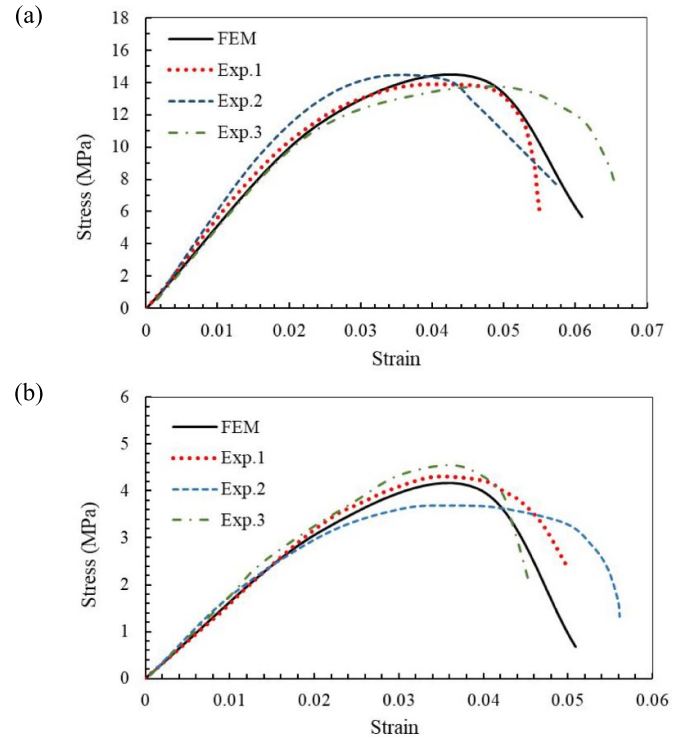


Figure 9. Stress–strain diagrams of SHPB dynamic loading: (a) Multiple-Arc and (b) RED auxetic samples.

Table 3. Experimental and FEM values of σ_u for Multiple-Arc and RED structures.

σ_u	Exp.	FEM	Error (%)
Multiple-Arc	13.89	14.47	7.19
	14.16		2.14
	13.73		5.11
RED	4.28	4.19	2.14
	3.72		11.21
	4.55		7.91

5.2. Mechanical performance of the designed structures under dynamic loading

In section 5.1, the FE simulations were validated with experiments. In this section, the mechanical performances of the designed structures are analyzed and compared. Figures 10 and 11 show the stress–strain diagrams and the deformations sequences of the designed structures under dynamic loading. Also, table 4 presents their EA, SEA and maximum Poisson's ratio values under dynamic loading.

According to figure 10 and table 4, the Multiple-Arc structure exhibits the highest EA and SEA, making it a promising auxetic configuration for EA. This can be attributed to the additional arc-shaped members which enhances its capacity to absorb impact energy under dynamic loading. Additionally, this structure demonstrates distinct strain hardening behavior as stress increases with strain. According to figure 10, in the second region of the curve, plastic deformation occurs, but the structure resists this deformation.

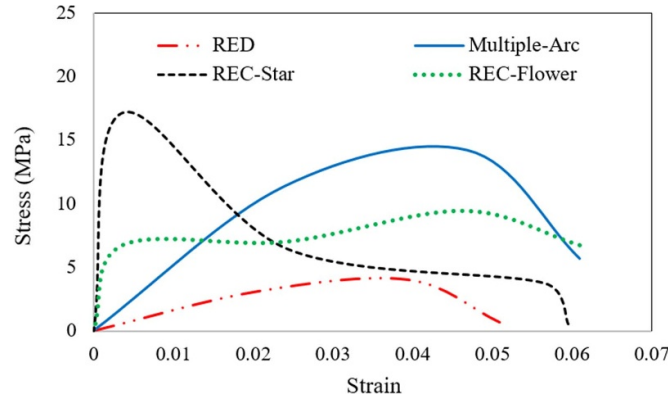


Figure 10. Stress–strain diagrams of the designed structures obtained from FE simulation of the SHPB.

Table 4. Values of EA, SEA, ν_{\max} , and ε_{\max} obtained from FE analysis.

Unit cell	EA (J/m^3) $\times 10^6$	SEA (J/kg) $\times 10^3$	ν_{\max}
RED	0.135	0.199	−1.55
Multiple-Arc	0.633	0.933	−1.11
REC-Star	0.424	0.625	−0.92
REC-Flower	0.473	0.697	−1.07

In contrast, the RED structure, due to the absence of internal members, lacks the ability to efficiently guide and transmit the impact-induced wave from the input bar to the output bar. As shown in figure 11(a), the lack of internal members significantly reduces wave transmission efficiency, leading to lower stress development and consequently a noticeable decrease in EA capacity.

Moreover, despite incorporating internal members that theoretically enhance wave transmission, the REC-Star and REC-Flower structures have not demonstrated the expected EA capacity. Their performance remains moderate compared to other configurations. According to figure 10, the REC-Star initially exhibits high EA capacity during the early stages of loading. However, the sharp corners in its design induces stress concentration, resulting in premature member failure and a sharp decline in load-bearing capacity. This abrupt failure is the primary factor contributing to the reduced EA efficiency of this structure. Furthermore, in the REC-Star, the stress–strain curve exhibits an abrupt drop after reaching the yield stress, indicating strain softening behavior. This behavior is due to the rapid change in load transfer path and the reconfiguration of the structural members after passing the yield region. At this stage, the internal members of the structure release part of the stored energy, leading to strain softening and a significant reduction in the structural resistance. This behavior results in a decrease in structural stiffness and a transition of the structure to a more stable state with lower stress, which appears as an abrupt drop in the stress–strain curve. In these structures, as strain increases, stress decreases, leading to a diminished capacity to resist higher stresses.

According to table 4, the arrangements of internal members directly affect the Poisson’s ratio value of the structures. The RED structure, due to its geometry and fewer members compared to other designed structures, has the maximum space for lateral deformation, resulting in the highest negative Poisson’s ratio value. In contrast, the REC-Star exhibits the lowest negative Poisson’s ratio among the structures. Its internal arrangement does not allow enough space for displacement during loading; hence, the presence of internal diagonal members reduces the negative Poisson’s ratio. Among the structures, the REC-Flower performs satisfactorily in terms of EA and the negative Poisson’s ratio, benefiting from more vacant space that allows lateral struts to be more flexible and experience greater deformation, leading to an increased negative Poisson’s ratio. However, this increased flexibility also reduces the structure’s resistance to axial impact, consequently lowering its EA capacity.

In summary, each designed configuration exhibits distinct mechanical properties, making them suitable for various engineering applications under dynamic loading. The Multiple-Arc structure provides the highest EA in a short time, making it ideal for impact-resistant designs and energy absorber devices. The RED structure exhibits the highest negative Poisson’s ratio, which may be beneficial in applications requiring auxetic behavior. Meanwhile, the REC-Star and REC-Flower structures exhibit effective EA under gradual deformation, making them suitable for scenarios where progressive energy dissipation is necessary.

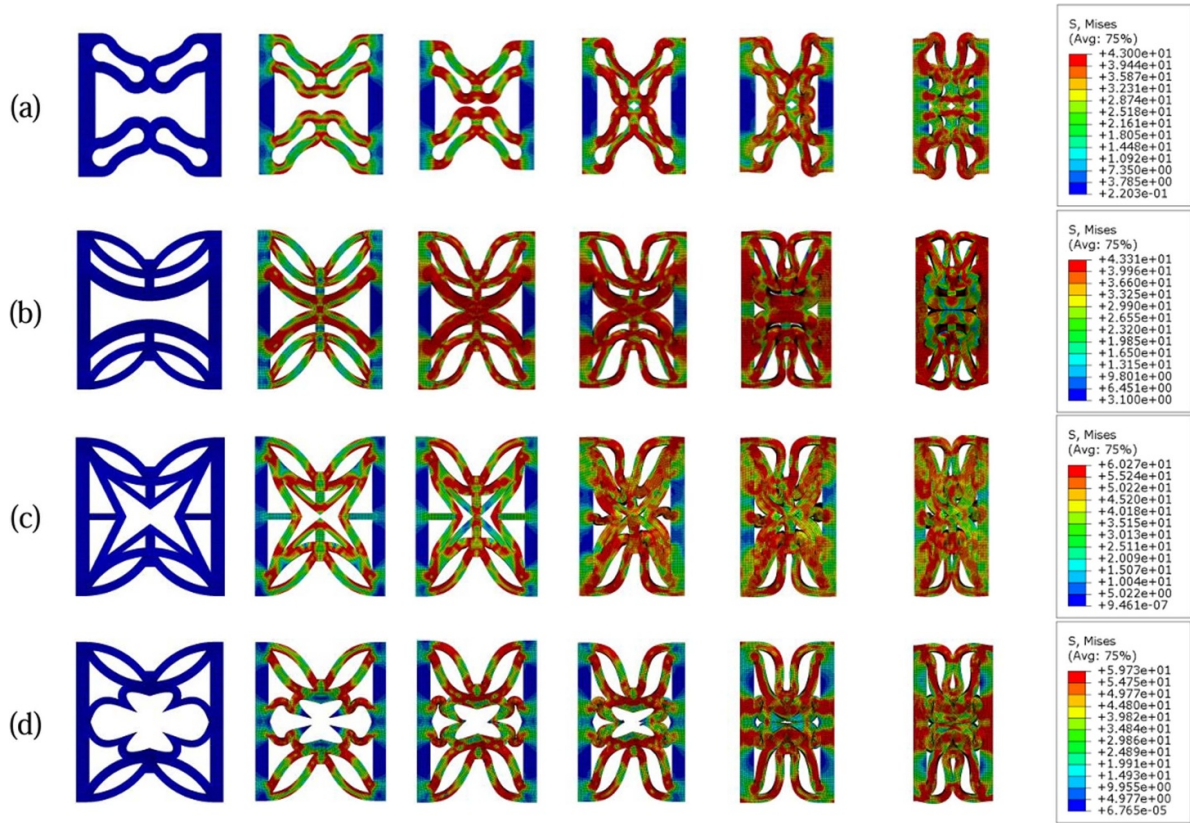


Figure 11. Deformation sequences of the structures under dynamic loading: (a) RED, (b) Multiple-Arc, (c) REC-Star, and (d) REC-Flower (the contours represent the final von Mises stress distribution).

6. Conclusions

This study examined the mechanical performance of several auxetic energy-absorbing structures under dynamic loading, using both experimental SHPB testing and FEM. The Multiple-Arc and RED structures were fabricated using FDM and tested experimentally, while all configurations were analyzed numerically. The validation results demonstrated strong agreement between experimental and numerical findings.

A comparative analysis of EA, SEA, and Poisson's ratio was conducted for all structures. The Multiple-Arc structure exhibited the highest EA and SEA due to its arc-shaped internal members, which facilitated efficient wave transmission and stress distribution. The REC-Flower structure also performed well, benefiting from curved members that minimized stress concentration. In contrast, the RED structure exhibited the lowest EA due to the absence of internal members, resulting in poor wave transmission. The REC-Star structure initially absorbed high energy but failed prematurely due to stress concentration at sharp corners. Additionally, Poisson's ratio analysis revealed that the RED structure exhibited the highest negative Poisson's ratio due to the auxetic nature of its Dumbell members and the increased space for lateral compression compared to other designed structures.

Here, is the key finding results of this study:

- Due to its arc-shaped internal members, the Multiple-Arc structure improved wave transmission and stress distribution, resulting in the highest EA.
- The REC-Flower structure showed favorable performance in reducing stress concentration thanks to its curved members.
- The RED structure's lack of internal members caused weak wave transmission and the lowest EA.
- The REC-Star structure, despite initially high EA, experienced early degradation due to stress concentration at sharp corners.

This research provides valuable insights into the design of auxetic structures for dynamic applications and paves the way for their potential use in areas such as crashworthiness, automotive and transportation, vibration damping in civil engineering structures, impact-resistant packaging, and advanced engineering systems.

In future work, geometrical parametric study and optimization of the Multiple-Arc structure, as the design with the highest EA, will be carried out to further enhance its performance and achieve the maximum NPR value. Additionally, this study is limited to a selected set of arc-shaped auxetic structures tested under Hopkinson impact

loading. Our future research will focus on geometry optimization to achieve maximum EA capability of arc-shaped auxetic structures via advanced optimization methods such as topology optimization.


Data availability statement

No new data were created or analysed in this study.

Acknowledgment

This work was supported by the Research Grants Council of Hong Kong Special Administrative Region Government under the NSFC/RGC Joint Research Scheme (Grant No: N_PolyU516/20).

Author contributions


Ehsan Etemadi  0000-0003-4382-0722
Conceptualization (equal), Methodology (equal),
Resources (equal), Writing – original draft (equal)

Mahbubeh Hosseinabadi
Data curation (equal), Formal analysis (equal),
Investigation (equal), Software (equal)

Mohaddeseh Gholikord
Formal analysis (equal), Investigation (equal),
Software (equal), Validation (equal)

Mohammad Abbaslou
Writing – original draft (equal)

Mohammad Imani
Resources (equal)

Hong Hu  0000-0002-5098-2415
Funding acquisition (equal), Project administration (equal),
Supervision (equal), Writing – review & editing (equal)

References

- [1] Mahdinejad Gorji J, Payganeh G and Moradi-Dastjerdi R 2024 Mechanical and energy absorption behavior of an innovative high-performance auxetic structure *Mech. Based Des. Struct. Mach.* **52** 2316–35
- [2] Etemadi E, Zamani A M M, Scarpa F, Zeeshan M, Hosseinabadi M and Hu H 2024 Modified re-entrant auxetic metamaterials with energy absorption enhancement *Mater. Today Commun.* **38** 108079
- [3] Zhang Y, Ren X, Han D, Cheng X, Jiang W, Zhang X G, Zhang X Y and Xie Y M 2022 Static and dynamic properties of a perforated metallic auxetic metamaterial with tunable stiffness and energy absorption *Int. J. Impact Eng.* **164** 104193
- [4] Khadem-Reza L, Etemadi E, Abbaslou M and Hu H 2022 Design of novel 3D auxetic structures based on S-shaped unit-cells *Smart Mater. Struct.* **31** 075024
- [5] Linforth S, Ngo T, Tran P, Ruan D and Odish R 2021 Investigation of the auxetic oval structure for energy absorption through quasi-static and dynamic experiments *Int. J. Impact Eng.* **147** 103741
- [6] Etemadi E, Hosseinabadi M, Taghizadeh M, Scarpa F and Hu H 2024 Enhancing the energy absorption capability of auxetic metamaterials through auxetic cells within re-entrant circular units *Eng. Struct.* **315** 118379
- [7] Etemadi E, Molla-Mohammad Zamani A R and Safikhani-Nasim M 2021 Experimental and numerical analysis of effective geometrical parameters for energy absorbing of the structures with negative Poisson's ratio made from aluminium alloy 1100 *J. Solid Fuels Mech.* **11** 311–24 (available at: https://jsfm.shahroodut.ac.ir/article_2160.html?lang=en)
- [8] Taghizadeh M, Gholikord M and Etemadi E 2025 Enhanced design and experimental validation of negative and zero Poisson's ratio metamaterials using topology optimization method *Smart Mater. Struct.* **34** 045018
- [9] Zhang M et al 2024 Low-velocity impact response of 3D carbon fiber reinforced polymer auxetic lattice structures *Polym. Compos.* **45** 7191–204
- [10] Etemadi E, Zhang M, Li K, Bashtani M, Po Ho M M, Tahir D and Hu H 2023 Load-bearing characteristics of 3D auxetic structures made with carbon fiber reinforced polymer composite *Compos. Struct.* **319** 117206
- [11] Etemadi E, Gholikord M, Zeeshan M and Hu H 2023 Improved mechanical characteristics of new auxetic structures based on stretch-dominated-mechanism deformation under compressive and tensile loadings *Thin-Walled Struct.* **184** 110491
- [12] Menon H G, Dutta S, Krishnan A, Mp H and Shankar B 2022 Proposed auxetic cluster designs for lightweight structural beams with improved load bearing capacity *Eng. Struct.* **260** 114241
- [13] Lu F, Wei T, Zhang C, Huang Y, Zhu Y and Rui X 2024 A novel 3D tetra-missing rib auxetic meta-structure with tension/compression-twisting coupling effect *Thin-Walled Struct.* **199** 111764
- [14] Kolken H, Garcia A F, Plessis A D, Meynen A, Rans C, Scheys L, Mirzaali M J and Zadpoor A A 2022 Mechanisms of fatigue crack initiation and propagation in auxetic meta-biomaterials *Acta Biomater.* **138** 398–409
- [15] Wagih A, Mahmoud H A and Lubineau G 2024 3D printed auxetic metal stiffener for lightweight metal-composite T-joints with high strength and toughness *Mater. Des.* **241** 112963
- [16] Zouaoui M, Saifouni O, Gardan J, Makke A, Recho N and Kauffmann J 2022 Improvement of fracture toughness based on auxetic patterns fabricated by metallic extrusion in 3D printing *Procedia Struct. Integr.* **42** 680–6
- [17] Yang S, Chalivendra V B and Kim Y K 2017 Fracture and impact characterization of novel auxetic Kevlar®/Epoxy laminated composites *Compos. Struct.* **168** 120–9
- [18] Chikkanna N, Krishnapillai S and Ramachandran V 2023 Investigation on the indentation performance of 3D printed re-entrant diamond auxetic metamaterial: printability and tailorability for futuristic applications *Rapid Prototyp. J.* **29** 1904–22
- [19] Parisi M, Allen T, Colonna M, Pugno N and Duncan O 2023 Indentation and impact response of conventional, auxetic, and shear thickening gel infused auxetic closed cell foam *Smart Mater. Struct.* **32** 074004
- [20] Li Z, Wang K and Wang B 2021 Indentation resistance of brittle auxetic structures: combining discrete representation and continuum model *Eng. Fract. Mech.* **252** 107824
- [21] Li T, Liu F and Wang L 2020 Enhancing indentation and impact resistance in auxetic composite materials *Composites B* **198** 108229
- [22] Hu J, Wang B L, Hirakata H and Wang K F 2023 Thermal shock fracture analysis of auxetic honeycomb layer based on non-Fourier heat conduction *Eng. Struct.* **279** 115581

- [23] Hu J, Wang B L, Li J E and Li Z 2022 Thermal shock resistance enhancement of auxetic honeycomb layer considering multi-cracking and temperature-dependent material properties *Int. J. Heat Mass Transf.* **135** 106072
- [24] Li Z, Wang B and Wang K 2021 Mechanism of crack initiation and propagation of re-entrant auxetic honeycombs under thermal shock *J. Appl. Mech.* **88** 111008
- [25] Hu J and Wang B 2021 Crack growth behavior and thermal shock resistance of ceramic sandwich structures with an auxetic honeycomb core *Compos. Struct.* **260** 113256
- [26] Bohara R P *et al* 2023 Anti-blast and-impact performances of auxetic structures: a review of structures, materials, methods, and fabrications *Eng. Struct.* **276** 115377
- [27] Etemadi E, Bashtani M and Hu H 2024 Novel auxetic metamaterials inspired from geometry patterns of an Iranian Mosque with improved energy absorption capability *Mater. Today Commun.* **41** 110470
- [28] Xu M, Xu Z, Zhang Z, Lei H, Bai Y and Fang D 2019 Mechanical properties and energy absorption capability of AuxHex structure under in-plane compression: theoretical and experimental studies *Int. J. Mech. Sci.* **159** 43–57
- [29] Zou Z, Xu F, Niu X, Fang T and Jiang Z 2023 In-plane crashing behavior and energy absorption of re-entrant honeycomb reinforced by arched ribs *Compos. Struct.* **325** 117615
- [30] Zhu X *et al* 2023 Design and energy absorption of star-shaped nesting cells and gradient lattice structures with negative Poisson's ratio effect *Mech. Adv. Mat. Struct.* **31** 1–15
- [31] Teng X C, Ren X, Zhang Y, Jiang W, Pan Y, Zhang X G, Zhang X Y and Xie Y M 2022 A simple 3D re-entrant auxetic metamaterial with enhanced energy absorption *Int. J. Mech. Sci.* **229** 107524
- [32] Safikhani Nasim M and Etemadi E 2017 Analysis of effective parameters of auxetic composite structure made with multilayer orthogonal reinforcement by finite element method *Mod. Mech. Eng.* **17** 247–54 (available at: https://mme.modares.ac.ir/browse.php?a_id=9635&sid=15&slc_lang=en)
- [33] Abbaslou M, Hashemi R and Etemadi E 2023 Novel hybrid 3D-printed auxetic vascular stent based on re-entrant and meta-trichiral unit cells: finite element simulation with experimental verifications *Mater. Today Commun.* **35** 105742
- [34] Zamani A M, Etemadi E, Bodaghi M and Hu H 2023 Conceptual design and analysis of novel hybrid auxetic stents with superior expansion *Mech. Mater.* **187** 104813
- [35] Ebrahimi M S, Noruzi M, Hamzehei R, Etemadi E and Hashemi R 2023 Revolutionary auxetic intravascular medical stents for angioplasty applications *Mater. Des.* **235** 112393
- [36] Shirzad M, Bodaghi M, Oh D, Yi M and Nam S Y 2024 Design and optimization of bioinspired auxetic structure for biomedical applications *Eur. J. Mech. A/Solids* **103** 105139
- [37] Park J H, Park H-J, Tucker S J, Rutledge S K, Wang L, Davis M E and Hollister S J 2023 3D printing of poly- ϵ -caprolactone (PCL) auxetic implants with advanced performance for large volume soft tissue engineering *Adv. Funct. Mater.* **33** 2215220
- [38] Jin Y, Xie C, Gao Q, Zhou X, Li G, Du J and He Y 2021 Fabrication of multi-scale and tunable auxetic scaffolds for tissue engineering *Mater. Des.* **197** 109277
- [39] Kim Y, Son K H and Lee J W 2021 Auxetic structures for tissue engineering scaffolds and biomedical devices *Materials* **14** 6821
- [40] Mogheiseh M, Etemadi E and Hasanzadeh Ghasemi R 2023 Design, molecular dynamics simulation, and investigation of the mechanical behavior of DNA origami nanotubes with auxetic and honeycomb structures *J. Biomol. Struct. Dyn.* **41** 1–10
- [41] Emerson R and Rhee J 2024 Analyzing auxetic cellular structures for personal protective gear designs *Int. Textile and Apparel Association Annual Conf. Proc.* (Iowa State University Digital Press)
- [42] Meeusen L, Candidori S, Micoli L L, Guidi G, Stanković T and Graziosi S 2022 Auxetic structures used in kinesiology tapes can improve form-fitting and personalization *Sci. Rep.* **12** 13509
- [43] Chen Z, Li J, Wu B, Chen X, Ren X and Xie Y M 2023 A novel bio-inspired helmet with auxetic lattice liners for mitigating traumatic brain injury *Smart Mater. Struct.* **32** 105020
- [44] Hanna B, Adams R, Townsend S, Robinson M, Soe S, Stewart M, Burek R and Theobald P 2021 Auxetic metamaterial optimisation for head impact mitigation in American football *Int. J. Impact Eng.* **157** 103991
- [45] Zeeshan M, Hu H and Etemadi E 2023 Geometric analysis of three-dimensional woven fabric with in-plane auxetic behavior *Polymers* **15** 1326
- [46] Kabir S, Li Y, Salahuddin M and Lee Y-A 2025 Drapability of 3D-printed auxetic structure textiles for wearable products through the digital image processing technique *Clothing Text. Res. J.* **43** 48–64
- [47] Luan K, Newman Z, West A, Lee K-L and Rokkam S 2023 Efficient Poisson's ratio evaluation of weft-knitted auxetic metamaterials *Textiles* **3** 275–86
- [48] Du Z, He L and Liu Z 2024 Design, preparation and characterization of braiding auxetic yarns with a high negative poisson's ratio *Text. Res. J.* **94** 82–89
- [49] Zeeshan M *et al* 2024 Three-dimensional auxetic woven fabric structure with in-plane negative poisson's ratio for composite reinforcement: a finite-element analysis *Text. Res. J.* **95** 00405175241299142
- [50] Lin L, Zhang H and Fan C 2024 The study on the properties of a metamaterial composed of star-shaped auxetic and curved-beam multi-stable structure *Mech. Adv. Mat. Struct.* **1–17**
- [51] Guo Z, Li Z, Li X, Mo Z and Li J 2023 Theoretical, numerical, and experimental study on quasi-static compressive behaviors of elliptical anti-chiral auxetic structure *Mater. Today Commun.* **34** 105059
- [52] Wang S and Liu H-T 2023 Energy absorption performance of the auxetic arc-curved honeycomb with thickness and arc angle gradient based on additive manufacturing *Mater. Today Commun.* **35** 105515
- [53] Wang M, Wu H, Yang L, Chen A, Chen P, Wang H, Chen Z and Yan C 2023 Structure design of arc-shaped auxetic metamaterials with tunable poisson's ratio *Mech. Adv. Mat. Struct.* **30** 1426–36
- [54] Qi C *et al* 2020 Quasi-static crushing behavior of novel re-entrant circular auxetic honeycombs *Composites B* **197** 108117
- [55] Luo W, Zhao T, Wang Z and Wang Z 2024 In-plane dynamic crushing of a novel arc-shaped reentrant structure *Mech. Adv. Mat. Struct.* **31** 8920–36
- [56] Zhang T, Huang Z, Li Y, Xu Z, Zhou Z and Chen Z 2023 Compressive mechanical behaviors of PPR and NPR chiral compression–twist coupling lattice structures under quasi-static and dynamic loads *Thin-Walled Struct.* **182** 110234
- [57] Solak K and Orhan S N 2023 Performance evaluation of peanut-shaped tubular auxetics with enhanced stiffness: a finite element study *Model. Simul. Mater. Sci. Eng.* **31** 015006
- [58] Etemadi E, Hosseinabadi M, Scarpa F and Hu H 2023 Design, FDM printing, FE and theoretical analysis of auxetic structures consisting of arc-shaped and dumbbell-shaped struts under quasi-static loading *Compos. Struct.* **326** 117602

- [59] Mauko A, Emre Yilmaz Y, Novak N, Doktor T, Vesenjak M and Ren Z 2024 Dynamic characterisation of novel three-dimensional axisymmetric chiral auxetic structure *Compos. Struct.* **333** 117949
- [60] Li Z-Y, Zhang W-M, Zou S, Wang X-T, Ma L, Wu L-Z and Hu H 2024 Quasi-static uniaxial compression and low-velocity impact properties of composite auxetic CorTube structure *Thin-Walled Struct.* **202** 112059
- [61] Solak K and Orhan S 2024 Quasi-static crashworthiness behaviour of auxetic tubular structures based on rotating deformation mechanism *Smart Mater. Struct.* **33** 15
- [62] Fu T, Wang X, Hu X and Rabczuk T 2024 Impact dynamic response of stiffened porous functionally graded materials sandwich doubly-curved shells with Arc-type auxetic core *Int. J. Impact Eng.* **191** 105000
- [63] Hao H *et al* 2024 In-plane deformation behavior and energy absorption characteristics of a straight-arc coupled auxetic metamaterial inspired by arch bridges *Structures* (Elsevier)
- [64] Hopkinson B 1914 X. A method of measuring the pressure produced in the detonation of high explosives or by the impact of bullets *Phil. Trans. R. Soc. Lond. A.* **213** 437–56
- [65] Kolsky H 1949 An investigation of the mechanical properties of materials at very high rates of loading *Proc. Phys. Soc. B* **62** 676
- [66] Etemadi E, Zhang M, Gholikord M, Li K, Mei Po Ho M and Hu H 2024 Quasi-static and dynamic behavior analysis of 3D CFRP woven laminated composite auxetic structures for load-bearing and energy absorption applications *Compos. Struct.* **340** 118182
- [67] Zhong J, Zhao C, Chen C, Lai W L and Wang Q 2025 Mechanical behaviors of composite auxetic structures under quasi-static compression and dynamic impact *Eur. J. Mech. A/Solids* **109** 105454
- [68] Mohan A, Mondal P and Rengaswamy J 2023 Impact behavior of auxetic structures: experimental and numerical analysis *Mater. Today Proc.* **87** 292–8
- [69] Ma Y, Zhao F, Liu J, Zhang Y, Xu Y, Zhang P, Gao S and Zhang J 2023 Dynamic mechanical properties, interface structure evolution and deformation behaviors of PVA-carbon fiber reinforced concrete with negative poisson's ratio design *Constr. Build. Mater.* **391** 131897
- [70] Fíla T, Koudelka P, Falta J, Šleichrt J, Adorna M, Zlámál P, Neuhäuserová M, Mauko A, Valach J and Jiroušek O 2021 Impact behavior of additively manufactured stainless steel auxetic structures at elevated and reduced temperatures *Adv. Eng. Mater.* **23** 2000669
- [71] Nazari Z, Ahmadi H, Liaghat G and Vahid S 2022 Investigation on the compressive properties of auxetic foams under different loading rates *Polym. Eng. Sci.* **62** 1720–30
- [72] Ma Y, Zhang Y, Wang P, Liu J, Zhang Z, Wang S, Gao Y and Li M 2024 Dynamic damage behavior of auxetic textile reinforced concrete under impact loading *J. Build. Eng.* **97** 110764
- [73] Fíla T, Zlámál P, Jiroušek O, Falta J, Koudelka P, Kytýř D, Doktor T and Valach J 2017 Impact testing of polymer-filled auxetics using split Hopkinson pressure bar *Adv. Eng. Mater.* **19** 1700076
- [74] Chen J, Tao W and Pang S 2021 Impact testing of 3D re-entrant honeycomb polyamide structure using split Hopkinson pressure bar *Appl. Sci.* **11** 9882
- [75] Varas D, Pernas-Sánchez J, Fjeldberg N and Martín-Montal J 2023 Experimental analysis at different loading rates of 3D printed polymeric auxetic structure based on cylindrical elements *Polym. Test.* **119** 107930
- [76] Chen W W and Song B 2010 *Split Hopkinson (Kolsky) Bar: Design, Testing and Applications* (Springer)
- [77] Etemadi E, Zamani J, Francesconi A, Mousavi M V and Giacomuzzo C 2014 A new set-up to investigate plastic deformation of face centered cubic metals in high strain rate loading *Mod. Appl. Sci.* **8** 94
- [78] Systèmes D 2022 *ABAQUS Documentation, Version 2022* (Dassault Systèmes Simulia Corp)
- [79] Zamani J *et al* 2014 Modeling of high velocity impact in sandwich beams with FGM core *Numerical Modeling of Materials under Extreme Conditions* pp 107–20
- [80] Etemadi E, Ashani J Z and Mousavi M V 2014 High strain rate and plastic deformation response of OFHC copper by finite element method *Adv. Mech. Eng.* **2014** 471–80 (available at: <https://www.airitilibrary.com/Article/Detail/P20151123004-201412-201511240017-201511240017-471-480>)
- [81] Gupta M K 2024 Dynamic responses of copper and impact velocity of split Hopkinson pressure bar strikers *Proc. Inst. Civ. Eng.* **176** 132–47
- [82] Al-Rifaie H, Movahedi N and Lim T-C 2025 Development of novel auxetic-nonauxetic hybrid metamaterial *Eng. Fail. Anal.* **175** 109559
- [83] Gao D, Wang S, Zhang M and Zhang C 2021 Experimental and numerical investigation on in-plane impact behaviour of chiral auxetic structure *Compos. Struct.* **267** 113922
- [84] Hosseinabadi M, Etemadi E, Serjouei A and Bodaghi M 2023 3D printed negative stiffness meta-structures with superior energy absorption and super-elastic shape-recovery features *Smart Mater. Struct.* **32** 034006